NANO LETTERS

2004
Vol. 4, No. 5
899−903

Plasmon Hybridization in Nanoparticle Dimers

P. Nordlander* and C. Oubre

Department of Physics and Astronomy, M.S. 61, Rice University, Houston, Texas 77005-1892

E. Prodan

Department of Physics, University of California, Santa Barbara, California 93106

K. Li and M. I. Stockman

Department of Physics and Astronomy, Georgia State University, Atlanta, Georgia 30303

Received February 27, 2004; Revised Manuscript Received March 30, 2004

ABSTRACT

We apply the recently developed plasmon hybridization method to nanoparticle dimers, providing a simple and intuitive description of how the energy and excitation cross sections of dimer plasmons depend on nanoparticle separation. We show that the dimer plasmons can be viewed as bonding and antibonding combinations, i.e., hybridization of the individual nanoparticle plasmons. The calculated plasmon energies are compared with results from FDTD simulations.

The optical properties of metallic nanoparticles are a subject of considerable experimental and theoretical interest.[1−7] Much of this attention is stimulated by the possibilities of using the large electromagnetic field enhancements associated with the excitations of nanoparticle plasmons to increase the cross section for spectroscopies such as Raman spectroscopy.[8] Recent experiments have shown enhancements as large as 10−14 orders of magnitude, enabling spectroscopic detections of a single molecule.[9−11]

Nanoparticle dimers are of considerable importance in this context because of the large electromagnetic field enhancements that can occur at their junctions when the surface plasmons are excited.[12] While nanoparticle dimers may not be the optimal structure for electromagnetic field enhancements, they serve as a simple prototypical model system for the study of the important physical factors underlying the electromagnetic field enhancements. The two major factors are believed to be the interaction of localized plasmons and the interference of the electromagnetic fields generated by these plasmons. The plasmonic properties of nanoparticle dimers have recently been investigated using a variety of methods.[13−19] Despite these studies, there is a lack of physical consensus of how the dimer plasmon modes depend on interparticle separation. For instance, in the case of high aspect ratio dimers, one study finds that the energy shifts of the dimer dipolar plasmon energies can be accounted for by a simple dipolar interaction,[16] while another study finds shifts that depend exponentially on the interparticle spacing.[17]

In this paper we apply the plasmon hybridization method to investigate the nature of the plasmons of nanoparticle dimers.[2,20] We show that the dimer plasmons can be viewed as bonding and antibonding combinations, i.e., hybridization of the individual nanoparticle plasmons. For large D, the shifts of the dipolar dimer plasmons essentially follow the interaction energy between two classical dipoles ($1/D^3$). As D becomes smaller, the shifts of the dipolar dimer plasmons become much stronger and vary much faster, with D due to the interaction and mixing with higher multipole oscillations.

In a recent paper, we have shown that calculating the energies of plasmon resonances of complex metallic nanoparticles is equivalent to calculating the electromagnetic interactions between plasmons of nanostructures of simpler geometry.[2] The plasmons of a complex nanoparticle result from hybridization of the plasmons of the individual nanoparticles. The strength of the hybridization depends on the geometry of the composite particle.

In the plasmon hybridization method, the conduction electrons are modeled as a charged, incompressible liquid sitting on top of a rigid, positive charge representing the ion cores. The ion cores are treated within the jellium approximation, so the positive charge n_0 is uniformly distributed within the particle's boundaries. This hydrodynamic limit is

10.1021/nl049681c CCC: $27.50
Published on Web 04/14/2004

justified by the fact that ab initio and classical calculations lead to the same plasmon energies for metallic nanoparticles larger than a few nanometers.[21] The plasmon modes are self-sustained deformations of the electron liquid. Because the liquid is incompressible, the only effect of such deformations is the appearance of a surface charge. For a single solid metallic sphere, the surface charge can be expressed as

$$\sigma(\Omega, t) = n_0 e \sum_{l,m} \sqrt{\frac{l}{R^3}} S_{lm}(t) Y_{lm}(\Omega) \tag{1}$$

where $Y_{lm}(\Omega)$ is a spherical harmonic of the solid angle Ω. The deformation amplitudes S_{lm} represent the new degrees of freedom. R is the radius of the sphere. The dynamics of the deformations is described by the following Lagrangian:[20]

$$L_S = \frac{n_0 m_e}{2} \sum_{l,m} [\dot{S}_{lm}^2 - \omega_{S,l}^2 S_{lm}^2] \tag{2}$$

where

$$\omega_{S,l} = \omega_B \sqrt{\frac{l}{2l+1}} \tag{3}$$

is the solid sphere plasmon resonance and

$$\omega_B = \sqrt{\frac{4\pi e^2 n_0}{m_e}}$$

is the bulk plasmon frequency. Dielectric effects coming either from embedding media or polarization of the ion cores can be included into the formalism.[20] Since the objective of this paper is to elucidate the nature of the plasmon resonances in dimers, we neglect effects that do not change the qualitative picture of the problem. However, we emphasize that the plasmon hybridization method leads to accurate values for the plasmon energies when dielectric effects are taken into account.[2,20]

When the overall size of the system is significantly smaller than the plasmon wavelength ($D + 2R < \lambda/4$), retardation effects can be neglected. In this limit the dynamics of the plasmons is determined by the instantaneous Coulomb interaction between the surface charges

$$V(D) = \int {R_1}^2 \, d\Omega_1 \int {R_2}^2 \, d\Omega_2 \frac{\sigma^1(\Omega_1)\sigma^2(\Omega_2)}{|\vec{r}_1 - \vec{r}_2|} \tag{4}$$

which is a function of the separation distance D between the centers of the spheres. If the polar axis is chosen along the dimer axis and a real representation is adopted for the spherical harmonics, the interaction is diagonal in azimuthal quantum number, m. Consequently, the plasmon modes corresponding to different values of m decouple. We simplify

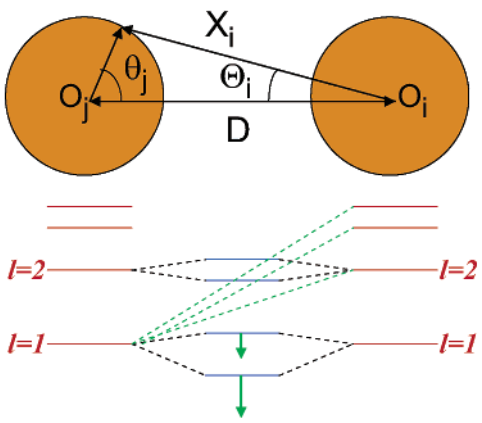

Figure 1. Schematic picture illustrating the plasmon hybridization in a nanoparticle dimer and the geometry of the problem. The individual nanosphere plasmons on the two particles interact and form bonding and antibonding dimer plasmons. In the dimer geometry, nanosphere plasmons with a given angular momentum l interact also with plasmons of different angular momentum on the other particle. This interaction induces extra shifts of the dimer plasmons at small separations. The figure illustrates this shift for the $l = 1$ derived dimer plasmons.

the formalism by introducing the subscript i to denote the noninteracting plasmon modes. In this notation, i refers to a plasmon mode of energy ω_i with angular momentum l_i on the nanosphere N_i of radius R_i. For a given azimuthal number m, the Lagrangian becomes

$$L^{(m)} = \frac{n_0 m_e}{2} \sum_{i,j} \left[(\dot{S}_i^2 - \omega_i^2 S_i^2)\delta_{ij} - \frac{\omega_B^2}{4\pi} V_{ij}^{(m)}(D) S_i S_j \right] \tag{5}$$

The interaction $V_{ij}^{(m)}$ is zero if i and j refer to the same sphere and

$$V_{ij}^{(m)}(D) = 4\pi \sqrt{l_i l_j R_i^{2l_i+1} R_j} \int d\theta_j \sin\theta_j \frac{P_{l_i}^m(\cos\Theta_i(\theta_j))}{(2l_i+1)X_i(\theta_j)^{l_i+1}} P_{l_j}^m(\cos\theta_j) \tag{6}$$

otherwise. In the above expression, the integration is over the surface of the particle N_j. The interaction matrix is symmetric, i.e., $V_{ij} = V_{ji}$. The geometry of the problem is illustrated in Figure 1. The quantity X_i is the distance between the center of particle N_i and a point on the surface of particle N_j of polar angle θ_j. The quantity Θ_i is the corresponding polar angle in the coordinate system of particle N_i. We note that the asymptotic form of the interaction between two sphere plasmon modes of angular momentum l, l' will vanish as $V \propto D^{-(l+l'+1)}$ or faster.

The Euler Lagrange equations result in an eigenvalue problem of the form

$$\det[A_{ij}^{(m)} - \omega^2] = 0 \tag{7}$$

where the matrix A is defined by

$$A_{ij}^{(m)} = \omega_i^2 \delta_{ij} + \frac{\omega_B^2}{8\pi}(V_{ij}^{(m)} + V_{ji}^{(m)}) \quad (8)$$

The structure of the secular equation is entirely analogous to the eigenvalue problem that describes how molecular levels form from atomic orbitals. The matrix elements V_{ij} describes the coupling (hybridization) between the modes i and j and results in separation dependent shifts of the dimer plasmon levels. The hybridization picture is illustrated in Figure 1. The relationship between dimer and individual nanoparticle plasmons and the analogy with molecular orbital theory has been suggested earlier,[13] but is here derived using a microscopic theory.

In the dimer calculations presented below, we consider the nanospheres being made of the same metal, described by an $r_s = 3$ and $\omega_B = 9$ eV. The calculations, which are fully converged for the present dimer separations, include sphere plasmons with angular momentum up to $l_{max} = 50$.

In Figure 2a, we show the dimer plasmon energies as a function of dimer separation for plasmon polarizations along the dimer axis ($m = 0$). At large separation, the plasmons on the different nanoparticles interact only weakly and the dimer plasmons are essentially bonding and an antibonding combinations of the nanoparticle plasmons of the same angular momentum l. In the following, we will use this asymptotic notation also when referring to the dimer plasmons for small separations, although the dimer plasmons in that case contain contributions from all angular momenta.

We now focus our attention on the lowest two dimer plasmons ($l = 1$) in Figure 2a. For large separations, the splitting of the bonding and antibonding dimer plasmons is symmetric. The splitting increases as their interaction increases, i.e., as $1/D^3$. The bonding configuration corresponds to the two dipole moments moving in phase (positive parity of dipole moments, or symmetric electric fields), and the antibonding configuration corresponds to the negative parity of the dipoles (antisymmetric fields). Since the net dipole moment of the negative parity (antisymmetric field) plasmons is zero for identical spheres, they are not easily excited by light and we will refer to them as dark plasmons in contrast to the positive parity (symmetric) plasmons, which will be referred to as bright (or luminous) plasmons. As the dimer separation decreases, the splitting of the $l = 1$ plasmons becomes asymmetric. It can be seen that the symmetric plasmon shifts downward in energy much faster than the antisymmetric $l = 1$ mode shifts upward. The antisymmetric plasmon shifts upward more slowly than expected from the dipole interaction $1/D^3$. This overall non-dipole-like red shift effect is caused by the interaction of the $l = 1$ nanosphere plasmons with higher l plasmons of the other nanosphere. This interaction involves higher powers of $1/D$. Panel (b) of the figure shows the $m = \pm 1$ plasmons, i.e., polarization oriented perpendicular to the dimer axis. The overall dependence of the dimer plasmon energies on dimer separation is similar to the $m = 0$ case. Since the dipole coupling for perpendicular polarizations has opposite sign, the assignment of dark and bright plasmons is reversed. The bright (symmetric) plasmons for $m = \pm 1$ are the antibonding

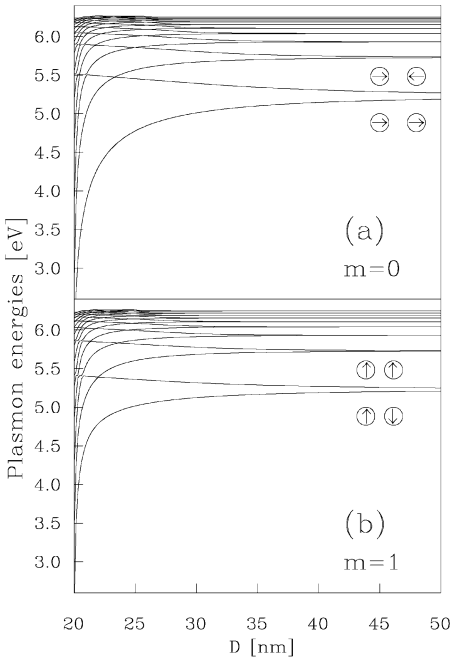

Figure 2. Calculated plasmon energies of a nanosphere dimer as a function of interparticle separation. The radius of the spheres is 10 nm. The electron density of the nanospheres corresponds to $r_S = 3.0$. Panel (a) is for $m = 0$ and (b) is for $m = 1$. The curves represent the bonding and antibonding dimer plasmons deriving from the individual nanosphere plasmons with increasing angular momentum l. The lowest energy curves are the plasmons that originate from the $l = 1$ plasmons. The orientation of their dipole moments is schematically indicated in the figures.

combinations of individual nanosphere plasmons. Our calculated dimer plasmon energies as a function of dimer separation are in perfect agreement with the results obtained using the full multipole calculations.[22]

In Figure 3, we show the calculated dimer plasmon energies for a heterodimer as a function of dimer separation. The radii of the nanospheres are 10 and 5 nm. In comparison with Figure 1, there are significant differences in the behavior with the separation. Since parity is broken, the dimer plasmon energies exhibit avoided crossings, i.e., the dimer plasmon modes repel each other. All dimer plasmons, both bonding and antibonding, with $|m| \leq 1$ are bright (those with $|m| = 2$ are dark; not shown in Figure 3). As the dimer distance changes through the avoided crossing, the symmetries of the dimer plasmons are exchanged. The interactions are particularly strong when antibonding plasmons approach the bonding dimer plasmons of higher l manifolds. The strong hybridization between the different l modes at small dimer separations means that also the higher l dimer plasmons will carry a finite dipole moment. Since both the bonding and antibonding dimer plasmons will be dipole-active, we expect the optical absorption spectra to display multiple peaks, or a broad absorption line in the case of overlapping resonances.

We show in the following how plasmon hybridization can be used to interpret the absorption spectra of dimers. For this we calculate their optical properties using the finite difference time domain (FDTD) method.[23] The FDTD method is fully retarded, but for the present small system, the electromagnetic fields are nearly dipole-like and can

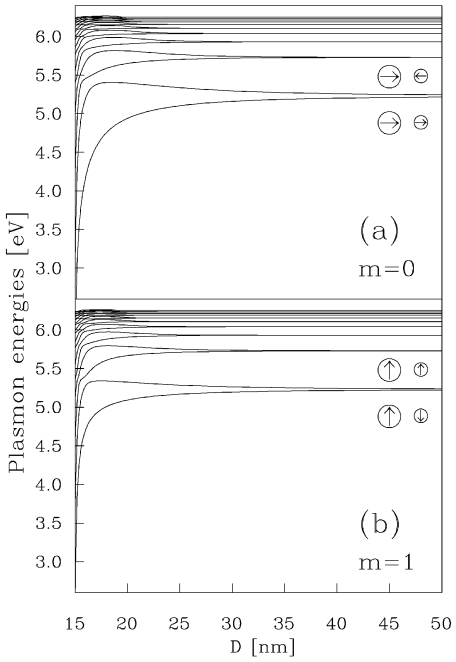

Figure 3. Calculated plasmon energies of a heterodimer as a function of interparticle separation. The radii of the spheres are 10 nm and 5 nm. The electron density is $r_S = 3.0$. Panel (a) is for $m = 0$ and (b) is for $m = 1$. The curves represent the bonding and antibonding dimer plasmons deriving from the individual nanosphere plasmons with increasing angular momentum l. The lowest energy curves are the plasmons that originate from the $l = 1$ plasmons. The orientation of their dipole moments are schematically indicated in the figures.

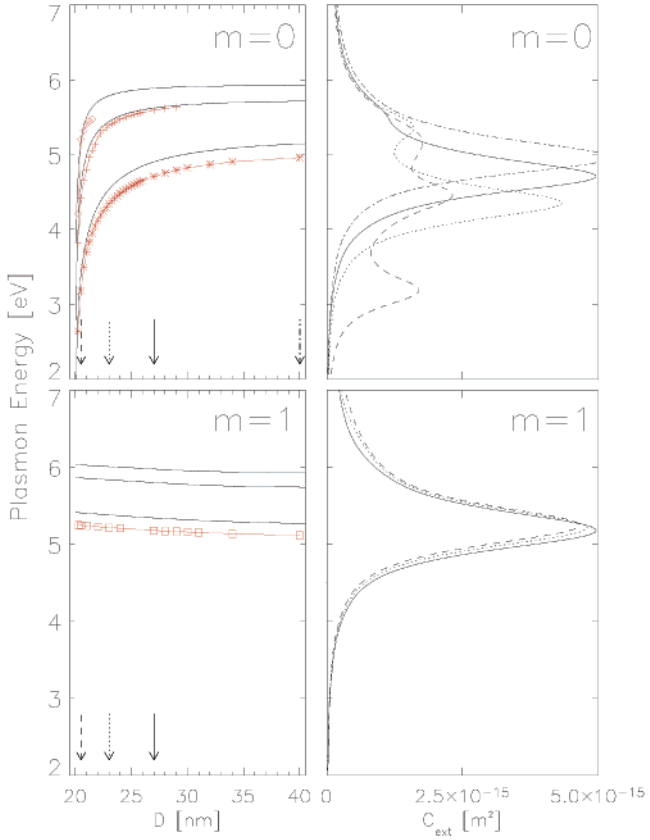

Figure 4. FDTD calculations of plasmon energies and extinction cross section spectra C_{ext} for nanosphere dimers of different separation D. The nanospheres are the same as in Figure 2. The upper panels refer to light polarized along the dimer axis ($m = 0$) and the lower panels are for perpendicular polarization ($m = \pm 1$). The right panels show the extinction cross section for separations $D = 20.5$ (dashed line), 23 (dotted line), 27 (solid line), and 40 nm (dash−dotted line). The left panels show the plasmon energies (energy of absorption peak maxima) as a function of dimer separation. For comparison, we include the plasmon energies for the three lowest bright plasmons (solid lines) obtained from the plasmon hybridization approach. The arrows indicate the dimer separations for which the extinction cross sections were calculated.

mostly couple to the dipole moments of the plasmons. To describe the dielectric function of the nanospheres, we use a Drude dielectric function for $r_S = 3$. A damping of 0.5 eV is introduced to improve the convergence of the calculations. This simple model dielectric function is used to enable a direct comparison with the results from the plasmon hybridization approach. For a more realistic modeling of the electromagnetic properties of nanoparticles, one would use experimentally measured dielectric functions.

The plasmon energies show up in the calculated extinction spectra as pronounced absorption peaks. The plasmon energies are obtained by fitting the peaks with Lorentzians. The upper left panels in Figure 4 show a comparison of the plasmon energies obtained from the FDTD simulations with those obtained using the plasmon hybridization method shown in Figure 2. The plasmon energies agree very well for all separations considered. For the present small systems, retardation effects are very small and the slight discrepancy for the $l = 1$ modes is caused by numerical errors in the FDTD simulations.[24] The upper right panel shows the calculated extinction cross section for $m = 0$ at the four distances indicated by arrows in the left panel. For the largest separation $D = 40$ nm, only one peak is visible in the extinction cross section. This is the bright $l = 1$ dimer plasmon. For $D = 27$ nm, the extinction spectra show two features: a pronounced dimer $l = 1$ peak at around 4.8 eV and weak shoulder from the dimer $l = 2$ plasmon at around 5.4 eV. For the present small system, the excitation fields are dipole-like and the dimer $l = 2$ plasmon is excited only because of its admixture of dipole-active $l = 1$ plasmons. At this relatively large separation, the hybridization is very weak. For the intermediate distance $D = 23$ nm, where the hybridization between $l = 1$ and $l = 2$ plasmons is larger, the spectra show two distinct peaks, corresponding to the dimer $l = 1$ and $l = 2$ plasmons. For the smallest separation $D = 20.5$ nm, the extinction spectra reveal three distinct peaks corresponding to the dimer $l = 1$, $l = 2$, and $l = 3$ plasmons. For this separation, these dimer plasmons are strongly hybridized and all contain a sizable admixture of dipole-active $l = 1$ modes. The lower panel shows the results for perpendicular polarization, $m = 1$. Here the interaction between the plasmons of different angular momentum l is smaller, resulting in less hybridization. Only the bright antibonding dimer $l = 1$ plasmon is visible.

In Figure 5, we show the result of the FDTD calculation for the heterodimer discussed in Figure 3. The organization of this figure is similar to Figure 4. The calculated dimer plasmon energies agree well with the results from the plasmon hybridization approach. The extinction cross sec-

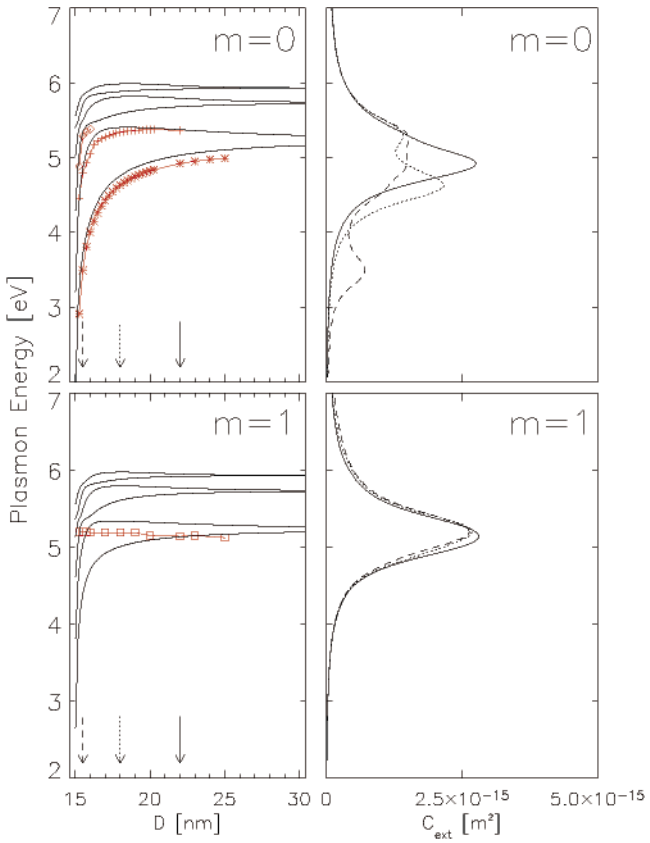

Figure 5. FDTD calculations of plasmon energies and extinction cross section spectra C_{ext} for nanosphere heterodimers of different separation D. The nanospheres are the same as in Figure 3. The upper panels refer to light polarized along the dimer axis ($m = 0$), and the lower panels are for perpendicular polarization ($m = \pm 1$). The right panels show the extinction cross section for separations $D = 20.5$ (dashed line), 23 (dotted line), and 27 nm (solid line). The left panels show the plasmon energies (energy of absorption peak maxima) as a function of dimer separation. For comparison, we include the plasmon energies for the six lowest dimer plasmons (solid lines) using the plasmon hybridization approach. The arrows indicate the dimer separations for which the extinction cross section were calculated.

tions are smaller for the heterodimer than for the homodimer because the number of electrons in the system is smaller. The upper panel shows the dimer plasmons for polarization parallel to the dimer axis $m = 0$. For $D = 27$ nm the extinction spectra display two features, the bonding and antibonding $l = 1$ plasmons. The antibonding $l = 1$ dimer plasmon is visible for the heterodimer because it has a net dipole moment. For the smallest separation, the two bonding and antibonding $l = 1$ and bonding $l = 2$ dimer plasmons are visible in the extinction cross section. The lower panel shows the results for the perpendicular polarization $m = \pm 1$. For this polarization, the splitting of the bonding and antibonding dimer plasmons is too small to be observed in the calculated extinction cross section spectrum.

We have shown that the plasmon hybridization method provides a detailed understanding of the energies and the extinction cross sections of the plasmons in a nanosphere dimer. The dimer plasmons can be viewed as bonding and antibonding linear combinations of individual nanosphere plasmons. As the dimer separation is decreased, individual sphere plasmons with different angular momentum hybridize, resulting in dimer plasmons with finite dipole moments.

Acknowledgment. This work was supported by the Multidisciplinary University Research Initiative of the Army Research Office (P.N.), the Robert A. Welch Foundation under grant C-1222 (P.N.,E.P.), the Texas Advanced Technology Program (P.N.,C.O.), the National Science Foundation under grants EIA-0216467 (P.N.), and EEC-0304097 (P.N.), the Chemical Sciences, Biosciences and Geosciences Division of the Office of Basic Energy Sciences, Office of Science, U.S. Department of Energy under grants DE-FG02-01ER15213 and DE-FG02-03ER15486 (M.S.), and by U.S.−Israel Binational Science Foundation (M.S.).

References

(1) Brongersma, M. L. *Nat. Mater*. **2003**, *2*, 296.
(2) Prodan, E.; Radloff, C.; Halas, N. J.; Nordlander, P. *Science* **2003**, *302*, 419.
(3) Barnes, W. L.; Dereux, A.; Ebbeson, T. W. *Nature* **2003**, *424*, 824.
(4) Aizpurua, J.; Hanarp, P.; Sutherland, D. S.; Kall, M.; Bryant, G. W.; de Abajo, F. J. G. *Phys. Rev. Lett*. **2003**, *90*, 57401.
(5) Sun, Y.; Xia, Y. *Science* **2002**, *298*, 2176.
(6) Jin, R.; Wei, Y.; Mirkin, C. A.; Kelly, K. L.; Schatz, G. C.; Zheng, J. G. *Science* **2001**, *294*, 1901.
(7) Bergman, D. J.; Stockman, M. I. *Phys. Rev. Lett*. **2003**, *90*, 027402.
(8) Moskovits, M.; Tay, L.; Yang, J.; Haslett, T. *Topics Appl. Phys*. **2002**, *82*, 215.
(9) Wang, Z.; Pan, S.; Krauss, T. D.; Dui, H.; Rothberg, L. J. *Proc. Nat. Acad. Sci. U.S.A*. **2003**, *100*, 8638.
(10) Nie, S.; Emory, S. R. *Science* **1997**, *275*, 1102.
(11) Michaels, A. M.; Nirmal, M.; Brus, L. E. *J. Am. Chem. Soc*. **1999**, *121*, 9932.
(12) Xu, H.; Bjerneld, E. J.; Kall, M.; Borjesson, L. *Phys. Rev. Lett*. **1999**, *83*, 4357.
(13) Gersten, J. I.; Nitzan, A. *Surf. Sci*. **1985**, *158*, 165.
(14) Schmeits, M.; Dambly, L. *Phys. Rev. B* **1991**, *44*, 12706.
(15) Tamaru, H.; Kuwata, H.; Miyazaki, H. T.; Miyano, K. *Appl. Phys. Lett*. **2002**, *14*, 348.
(16) Rechberger, W.; Hohenau, A.; Leitner, A.; Krenn, J. R.; Lamprecht, B.; Aussenegg, F. R. *Optics Comm*. **2003**, *220*, 137.
(17) Su, K. H.; Wei, Q. H.; Zhang, X.; Mock, J. J.; Smith, D. R.; Schultz, S. *Nano Lett*. **2003**, *3*, 1087.
(18) Futamata, M.; Maruyama, Y.; Ishikawa, M. *J. Phys. Chem. B* **2003**, *107*, 7607.
(19) Prikulis, J.; Svedberg, F.; Kall, M.; Enger, J.; Ramser, K.; Goksor, M.; Hanstorp, D. *Nano Lett*. **2004**, *4*, 115.
(20) Prodan, E.; Nordlander, P. *J. Chem. Phys*. **2004**, *120*, 5444.
(21) Prodan, E.; Nordlander, P. *Nano Lett*. **2003**, *3*, 543.
(22) Li, K.; Stockman, M. I.; Bergman, D. J. *Phys. Rev. Lett*. **2003**, *91*, 227402.
(23) Oubre, C.; Nordlander, P. *Proc. SPIE* **2003**, *5221*, 133.
(24) The slight numerical error is caused by the finite size discretization of space. Although the FDTD method is second order in the spatial grid,[25] our use of a Cartesian grid for simulating nonconforming systems introduces a first-order error.[26] Both of these errors vanish with infinitesimal grid resolutions. Differences between FDTD and plasmon hybridization are consistent in magnitude and direction with differences between FDTD and classical Mie theory. Calculations with a finer grid for selected distances reveals almost perfect agreement between the FDTD and the plasmon hybridization method.
(25) Taflove, A.; Hagness, S. C. *Computational Electrodynamics: The finite-difference time domain method*; Artech House: Norwood, MA, 2000.
(26) Ditkowski, A.; Dridi, K.; Hesthaven, J. S. *J. Comput. Phys*. **2000**, *170*, 39.

NL049681C